Article:
Smith, C.C. orcid.org/0000-0002-0611-9227 and Gilbert, M. orcid.org/0000-0003-4633-2839 (2022) The stress function basis of the upper bound theorem of plasticity. International Journal of Solids and Structures, 244-245. 111565. ISSN 0020-7683

https://doi.org/10.1016/j.ijsolstr.2022.111565

The stress function basis of the upper bound theorem of plasticity

Colin C. Smith[a,1,*], Matthew Gilbert[a]

[a]*Department of Civil and Structural Engineering, University of Sheffield, Sir Frederick Mappin Building, Mappin Street, Sheffield S1 3JD, UK*

Abstract

The discontinuous slip-line form of upper bound plasticity analysis is considered using an equilibrium of forces approach. It is demonstrated that the underlying basis of the approach can be written in terms of stress functions that provide a continuum stress state interpretation of the upper bound solution. An alternative proof of the upper bound theorem, applicable to both associative and non-associative materials, using stress functions is presented. The broader nature of the equilibrium form and the strict conditions under which it is valid are discussed, including examination of the apparent omission of moment equilibrium and associativity in many equilibrium form solutions. Finally, the relationship of the stress function formulation to the output of the computational limit analysis method discontinuity layout optimisation (DLO) and the potential to use the stress function formulation to derive a form of lower bound solution from an upper bound analysis are demonstrated.

Keywords: plasticity, limit analysis, upper bound, stress function

*Corresponding author

Email address: c.c.smith@sheffield.ac.uk (Colin C. Smith)

[1]Tel: +44 114 2225717, Fax: +44 114 2225700

1. Introduction

1.1. Background

The upper bound theorem of plasticity provides a long established and highly effective means of bounding the ultimate load carrying capacity of a mechanical system formed of ideal plastic materials and has a wide range of engineering applications, e.g. metal forming and cutting, geotechnical collapse, concrete and steel frame strength analysis.

The upper bound theorem of plasticity was first presented by Gvozdev (1938) and then separately by Hill (1951), and further extended by Drucker et al. (1952) and Collins (1969). The method traditionally involves postulating a compatible collapse mechanism consistent with the boundary conditions and using the equivalence of rate of external and internal energy dissipation to compute the ultimate load, or 'load factor'. Using the principle of virtual work this load can be proven to be an upper bound to the exact collapse load factor for an ideal plastic material, where such a material possesses a convex yield surface and an associative flow rule (where the strain increment is normal to the yield surface). Such a mechanism can utilise continuum velocity fields and/or discontinuous slip-lines/surfaces separating rigid zones.

While the energy or kinematic formulation of the upper bound theorem is most often covered in textbooks (e.g. Johnson and Mellor 1962, Calladine 1985, Chakrabarty 2006) and has sometimes been regarded as the 'pure' upper bound form, the equilibrium (equilibrium of forces) form of the upper bound theorem (sometimes referred to as a 'limit equilibrium' or LE form) has often been considered the 'lesser' form. Michalowski (1989) asserts that

the 'limit equilibrium' form is not equivalent to the energy balance limit analysis form of the upper bound theorem, and that the latter requires an associative flow rule, while the former does not. In this paper it will be shown that with the adoption of maximization, the two methods are in fact equivalent.

To the authors' knowledge no in depth study of the classical equilibrium approach has been presented. This paper re-examines the upper bound theorem in both kinematic and equilibrium form with specific focus on plane strain discrete slip-line fields, providing an alternative and novel mathematical proof based on the use of stress functions and applicable to both associative and non-associative materials. This provides a convenient framework to clarify the correct application of the equilibrium method and to provide new perspectives on the issue of apparent lack of moment equilibrium in many analyses in the equilibrium form, to examine issues related to non-associative problems, and to demonstrate how lower bound solutions may be derived using the same methodology as used to derive an upper bound. For simplicity the work will be restricted to the use of the Tresca or Mohr-Coulomb yield criteria and plane strain problems. However the principles discussed herein should apply to any convex yield function and may be extended to three dimensions.

In part this work builds on the principle of the mathematical duality of the kinematic and equilibrium forms in optimization. The principle of duality in optimization has long been established (e.g. Charnes et al. 1959. in the context of the limit analysis of trusses) and has been discussed e.g. by Ciria et al. (2008) in the context of continuum limit analysis and by Smith and

Gilbert (2007) in the context of discrete limit analysis via discontinuity layout optimization (DLO). This paper develops equations similar to those derived by Smith and Gilbert (2007). However in that work the wider significance of these equations was not discussed. The present work adopts a very different starting point and analytical framework that elucidates the underlying stress function basis of the approach from first principles.

1.2. Lower and upper bound theorems for associative materials

While the focus of this paper is the upper bound, it is convenient to restate both the conventional lower bound and upper bound theorems of plasticity as follows (after Chen 1975) for a problem involving an ideal plastic material possessing a convex yield surface and following an associative flow rule:

Theorem 1. ***(lower bound - associative material)*** *- If an equilibrium distribution of stress covering the whole body can be found which balances the applied loads on the stress boundary and is everywhere below yield then the body at the applied loads will not collapse.*

Theorem 2. ***(upper bound - associative material)*** *- If a compatible mechanism of plastic deformation is assumed, then the applied loads determined by equating the rate at which external forces do work to the rate of internal energy dissipation will either be higher or equal to the actual limit load.*

1.3. Theoretical issues arising from the equilibrium analysis approach

This paper will make extensive use of a simple punch indentation problem (common to e.g. soil and metal plasticity problems) involving a weightless

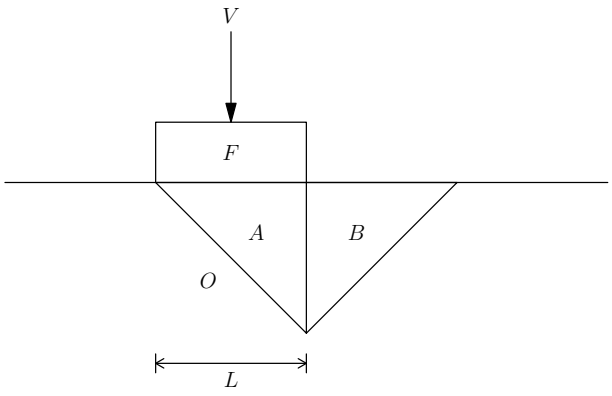

Figure 1: Simple analysis of the vertical indenter force V required to cause failure in a cohesive material

Tresca material of shear strength k to illustrate a number of theoretical issues. The simple postulated mechanism in Figure 1 can be used to illustrate use of the energy and equilibrium approaches to solve the indentation problem. Details of the kinematic energy calculation are presented in Appendix A, which gives the collapse load to be $V = 6kL$.

For the classical equilibrium method, the solution proceeds as follows. Free body diagrams are drawn with the direction of shear stress selected by inspection or by reference to the kinematic solution hodograph, as shown in Figure 2. Since shear failure is assumed to be occurring across interfaces OA, OB and AB, the following equations may be written:

$$S_A = S_B = \sqrt{2}kL \tag{1}$$

$$S = kL \tag{2}$$

Resolving forces for block B vertically and horizontally:

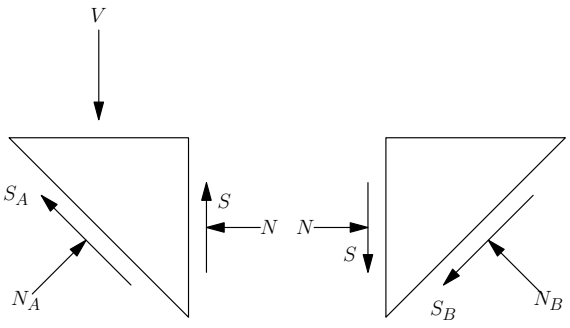

Figure 2: Free body diagrams for mechanism depicted in Figure 1

$$S + \frac{S_B}{\sqrt{2}} = \frac{N_B}{\sqrt{2}} \tag{3}$$

$$N = \frac{S_B}{\sqrt{2}} + \frac{N_B}{\sqrt{2}} \tag{4}$$

Hence

$$N = S + \sqrt{2}S_B = 3kL \tag{5}$$

Resolving forces for block A vertically and horizontally:

$$V = S + \frac{S_A}{\sqrt{2}} + \frac{N_A}{\sqrt{2}} \tag{6}$$

$$N + \frac{S_A}{\sqrt{2}} = \frac{N_A}{\sqrt{2}} \tag{7}$$

Hence

$$V = \sqrt{2}S_A + S + N = \sqrt{2}S_A + 2S + \sqrt{2}S_B = 6kL \tag{8}$$

which, as expected, is the same result as from the kinematic analysis. However five aspects of this analysis should be highlighted for further consideration:

1. The direction of shear stress acting on each boundary was determined intuitively or from the hodograph. (Appendix B provides an illustrative example of how an intuitive choice may not match the requirement for an upper bound).
2. Yield was assumed on each boundary.
3. At no stage was moment equilibrium considered.
4. There is no immediately apparent need that the arrangement of sliding blocks is able to form a kinematically compatible mechanism.
5. At no point was the associative flow rule explicitly considered.

These issues will be revisited later in the paper. The upper bound will now be examined from an alternative standpoint.

2. Methodology

2.1. Alternative upper bound theorem for associative and non-associative materials

An alternative proof of the upper bound theorem is given here which applies to a material with any flow rule, including non-associative flow rules:

Theorem 3. ***(upper bound - associative or non-associative material)*** *- If an equilibrium stress field is found, also in equilibrium with external forces such that the maximum possible load sustainable by the system*

is achieved without yield being violated in any part of the domain, then the applied load will be an upper bound to any collapse load.

This must hold since any increment of load would lead to stresses that would have to exceed yield in the domain to preserve equilibrium and thus an impossible state. While at first sight this theorem resembles the lower bound theorem (Theorem 1), the key differences here that renders it an upper bound, are: (i) the stipulation that a maximum load must be found (involving an exhaustive search of all possible equilibrium stress fields), and (ii) the absence of any conditions on the flow rule. Of course if an associative flow rule is adopted this then is also simultaneously a lower bound and the stipulation that the maximum possible load must be found, renders it a true plastic solution. However, it is rendered an upper bound in general since non-associative collapse mechanisms must occur at the same or lower loads (Chen, 1975).

The relative status of upper and lower bound solutions for both associative and non-associative materials can be usefully illustrated by the diagram in Figure 3. . It can be seen that for an associative material the optimal (lowest) upper bound equals the optimal (highest) lower bound and this gives a single unique true solution (in terms of collapse load - there may be multiple solutions that all give the same collapse load), whereas, for non-associative materials there is a range of true solutions. Here a true solution (for both associative and non-associative materials) is defined as one in which yield is not violated at any point and where application of the flow rule to the stress field results in a kinematically admissible velocity field that satisfies the velocity boundary conditions.

Non-associative true solutions are always less than or equal to the associative true solutions. It follows that the associative upper bounds are also upper bounds to non-associative materials. Lower bounds for non-associative Mohr-Coulomb materials may be determined by substituting the angle of dilation for the angle of shearing resistance in Theorem 1 (Chen, 1975). However these non-associative lower and upper bounds are not necessarily true solutions when optimised. . Only a very few examples of rigorous closed form true non-associative solutions exist for continuum materials, e.g. Smith (2012). whereas for discontinuous problems such as fractured rock and masonry, where potential failure lines are clearly pre-defined, non-associative results are readily available e.g. Gilbert et al. (2006). Non-associative true solutions may also be generated using incremental elasto-plastic finite element methods.

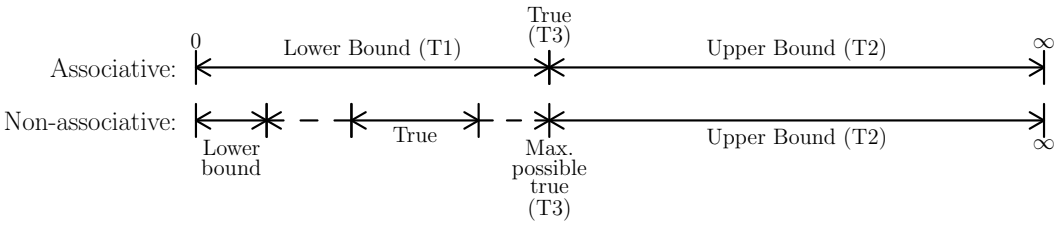

Figure 3: Relationship between associative and non-associative limit loads. T1, T2 and T3 refer to Theorems 1, 2 and 3 in the text.

An extension to Theorem 3 where only part of the domain is constrained can also be stated:

Theorem 4. ***(upper bound - associative or non-associative material)*** *- If an equilibrium stress field is found, also in equilibrium with ex-*

ternal forces such that the maximum possible load sustainable by the system is achieved without yield being violated in only part of the domain, then the applied load will be an upper bound to any collapse load.

This follows directly from Theorem 3. Checking more of the domain will, in general, improve the upper bound estimate. It is possible to undertake the checks either at points, along lines, or within elements. However it is necessary, but not necessarily sufficient, that the points, lines, and/or elements must form at least a continuous 'barrier' between the load and any support if the solution is not to be infinite (it will always be possible to find a stress state that bypasses unconnected points, lines or elements to result in an infinite load capacity when the load is maximised). Hence in Figure 1 the slip-lines separate the load from the (implicit) support at infinity in order to provide a potentially useful solution for e.g. a Tresca material. However it is known for example that the set of lines depicted in Figure 1 generate an infinite solution for any Mohr-Coulomb material with friction angle $\phi > 22.5^o$. Additionally, any 'free' ended line or element (i.e. one that does not form part of a continuous 'barrier') is redundant. Stresses in the parts of the domain between lines or elements that are not checked may exceed yield, thus giving rise to an upper bound solution. Since a continuous 'chain' of points leads to a line or element, only lines or elements need to be considered. In this paper consideration will be restricted to lines, consistent with classical rigid-block analysis. It is necessary therefore to consider the state of stress and yield along lines in an arbitrary stress field. This can be formulated in plane strain by considering an Airy stress function (Airy, 1863) and mechanisms involving a series of connected lines, furnishing a range of useful

outcomes.

2.2. Airy stress function

The use of stress functions has been a feature of many classical analysis approaches in continuum elasticity and in some areas of plasticity analysis, such as for torsion problems, e.g. Chakrabarty (2006), and in the lower bound analysis of concrete disks (Nielsen and Hoang, 2011). However the significance of such stress function solutions does not seem to have been considered for upper bound plasticity approaches.

Consider that a stress function field is sought, in equilibrium with external forces, that provides an upper bound solution to a problem defined by a series of lines (such as depicted in Figure 1). Moment and translational equilibrium is implicit, satisfying Theorem 4. Ensuring yield is not violated along each of the lines or rigid block boundaries while maximising the load then completes the application of the theorem. The theory enabling this process may be developed as follows.

The equations of equilibrium in two dimensions with body forces F_x and F_y acting in the +ve axes direction are given by:

$$\frac{\partial \sigma_x}{\partial x} + \frac{\partial \tau_{yx}}{\partial y} + F_x = 0 \tag{9}$$

and

$$\frac{\partial \sigma_y}{\partial y} + \frac{\partial \tau_{xy}}{\partial x} + F_y = 0 \tag{10}$$

$$\tau_{xy} = \tau_{yx} \tag{11}$$

Adopting the sign convention in Figure 4, where tension, anti-clockwise (τ_{xy}) shear stresses, and clockwise (τ_{yx}) shear stresses are all taken as positive, an arbitrary function Φ is defined such that:

$$\sigma_x = \Omega + \frac{\partial^2 \Phi}{\partial y^2} \tag{12}$$

$$\sigma_y = \Omega + \frac{\partial^2 \Phi}{\partial x^2} \tag{13}$$

$$\tau_{xy} = \tau_{yx} = -\frac{\partial^2 \Phi}{\partial x \partial y} \tag{14}$$

where the body forces are determined by the potential function Ω as:

$$F_x = -\frac{\partial \Omega}{\partial x} \tag{15}$$

$$F_y = -\frac{\partial \Omega}{\partial y} \tag{16}$$

It is found that the equations of equilibrium are identically satisfied for all values of Φ and Ω.

It is convenient for later derivations to define functions u, and v as follows:

$$u = \frac{\partial \Phi}{\partial y} \tag{17}$$

$$v = -\frac{\partial \Phi}{\partial x} \tag{18}$$

where the negative sign in equation (18) is adopted for consistency with the DLO formulation described in (Smith and Gilbert, 2007).

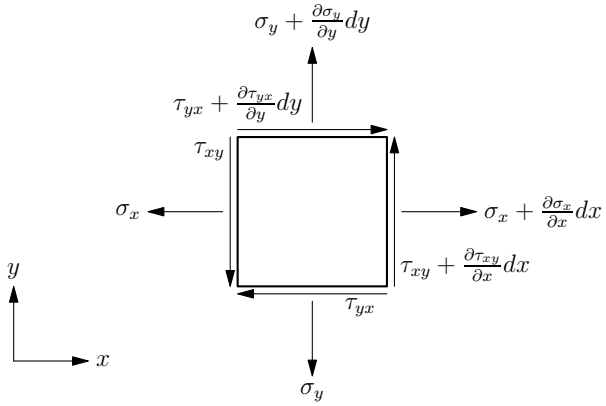

Figure 4: Conventional sign convention (tension positive)

2.3. Derivation of forces along a line

2.3.1. Basic equations

Consider a straight line joining two nodes a and b as shown in Figure 5, Given values of u, v, and Φ at these nodes and generalising the analysis of a specific case given by Airy (1863), the shear force S (clockwise positive), normal force N (tensile positive) and moment M (positive bending towards a) along any line can be computed.

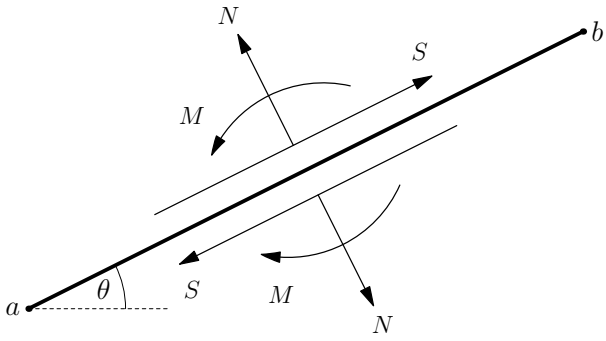

Figure 5: Forces along a discontinuity.

It is convenient to derive the stress function on a rotated coordinate system. Let α and β be direction cosines of the line where $\alpha = \cos\theta$ and $\beta = \sin\theta$ and where θ is the anti-clockwise angle of the line to the horizontal x-axis. It can be shown (see Appendix A) that shear and normal stresses along the line can be expressed as follows:

$$\tau = -\alpha\frac{du}{dl} - \beta\frac{dv}{dl} \tag{19}$$

$$\sigma_n = \beta\frac{du}{dl} - \alpha\frac{dv}{dl} \tag{20}$$

Hence the shear and normal forces along the line can be computed by integration as follows.

2.3.2. Shear and normal forces

$$S = \int_a^b \tau.dl = \int_a^b \left(-\alpha\frac{du}{dl} - \beta\frac{dv}{dl}\right).dl \tag{21}$$

$$S = \left[-\alpha u - \beta v\right]_a^b = -\alpha(u_b - u_a) - \beta(v_b - v_a) \tag{22}$$

$$N = \int_a^b \sigma_n.dl = \int_a^b \left(\beta\frac{du}{dl} - \alpha\frac{dv}{dl}\right).dl + \int_a^b \Omega.dl \tag{23}$$

$$N = \left[\beta u - \alpha v\right]_a^b = \beta(u_b - u_a) - \alpha(v_b - v_a) + \int_a^b \Omega.dl \tag{24}$$

where u_a, u_b, v_a, v_b are the values of u and v at nodes a and b. Hence the normal and shear forces can be determined by the values of u and v at the end points only and an integral of the body force function Ω.

2.3.3. Moment

The moment M about the midpoint of the line (m) can be similarly calculated as follows:

$$M = \int_a^b \sigma_n (l - l_m).dl = \int_a^b \left(\beta \frac{du}{dl} - \alpha \frac{dv}{dl}\right)(l - l_m).dl + M_\Omega \tag{25}$$

where $M_\Omega = \int_a^b \Omega(l - l_m).dl$, hence,

$$M = \int_a^b (\beta.du - \alpha.dv)(l - l_m) + M_\Omega \tag{26}$$

Integrating by parts gives:

$$= \beta \left([(l - l_m)u]_a^b - \int_a^b u.dl \right) - \alpha \left([(l - l_m)v]_a^b - \int_a^b v.dl \right) + M_\Omega \tag{27}$$

$$= \beta \left([(l - l_m)u]_a^b \right) - \alpha \left([(l - l_m)v]_a^b \right) - \int_a^b (\beta u - \alpha v).dl + M_\Omega \tag{28}$$

Noting (see Appendix C)

$$\Phi = \int (-v.\alpha + u.\beta).dl \tag{29}$$

gives:

$$= \beta \left([(l_b - l_m)u_b] - [(l_a - l_m)u_a] \right) - \alpha \left([(l_b - l_m)v_b] - [(l_a - l_m)v_a] \right) - (\Phi_b - \Phi_a)) + M_\Omega \tag{30}$$

$$M = -0.5\alpha l(v_a + v_b) + 0.5\beta l(u_a + u_b) + \Phi_a - \Phi_b + M_\Omega \tag{31}$$

where Φ_a, Φ_b are the values of Φ at nodes a and b. Moments may thus be derived from a knowledge of Φ and u and v at the end points and an integral of the body force function Ω. To some extent equations 22 and 24 share similarities to the nodal force theory employed in yield line analysis (Johansen, 1962), (Nielsen and Hoang, 2011); however these were derived for an out-of-plane analysis without reference to stress functions and do not address the additional moment calculations required in an in-plane analysis.

2.4. Checking yield violation on a line

To generate an upper bound solution that satisfies Theorem 4, it is necessary to demonstrate that yield is not violated on at least part of each line.

This may be achieved through the computation of S, N and M on each line, in combination with the yield function

$$f(S, N, M) = 0 \tag{32}$$

where f represents the yield function in an average sense.

In the following discussion, for clarity, the straight line joining the two end points a and b on which S, N and M are computed will now be termed the 'chord' between these points. In order to test for yield in an upper bound sense, it necessary to consider a specific family of 'slip-line' curves that also join these two points, forming a body between the curve and the chord. This curve must have a geometry that allows unknowns in the problem to be eliminated, in order that a generally applicable equation can be written.

Thus to generate a robust criterion using the Mohr-Coulomb yield criterion for example, it is necessary to utilise a suitable curve (a log spiral) such

that the resultant of the frictional shear, τ_ϕ and normal, σ_n, yield stresses (excluding those due to cohesion, τ_k) acts through a common centre as depicted in Figure 6 for a material with constant friction angle ϕ, where the total shear stress $\tau = \tau_k + \tau_\phi$. Taking moments about O it is thus necessary to balance only the moments due to M, N and S with the integral of the cohesive stresses acting along the curve, and the moment M_S due to the body forces acting on the segment between the chord and the curve. This must be demonstrated for all possible curve sets. The direction in which the shear stress acts is determined by the direction of relative rotation (ω) across the curve. The yield condition along the curve therefore becomes, for positive ω:

$$Stl + Nul + M \leq \int_a^b kr^2.d\psi + M_S \tag{33}$$

and for negative ω, where ul also becomes negative

$$-Stl - Nul - M \leq \int_a^b kr^2.d\psi + M_S \tag{34}$$

where it is necessary to consider rotation in either direction. For a constant angle of friction ϕ, in effect it is being shown that, on average:

$$\tau = \tau_k + \tau_\phi \leq k + \sigma_n \tan\phi \tag{35}$$

where the choice of curve enforces $\tau_\phi = \sigma_n \tan\phi$ and hence it remains to enforce $\tau_k \leq k$ along the line in an average sense (where τ_k may be less than zero). Thus it is not necessary to know the normal and shear stresses at every point along the line. This is a partial enforcement of yield, and hence satisfies Theorem 4, which is satisfied if $\tau_k \leq k$ everywhere but can be satisfied if $\tau_k \leq k$ on part of the line and $\tau_k > k$ on other parts. In either case

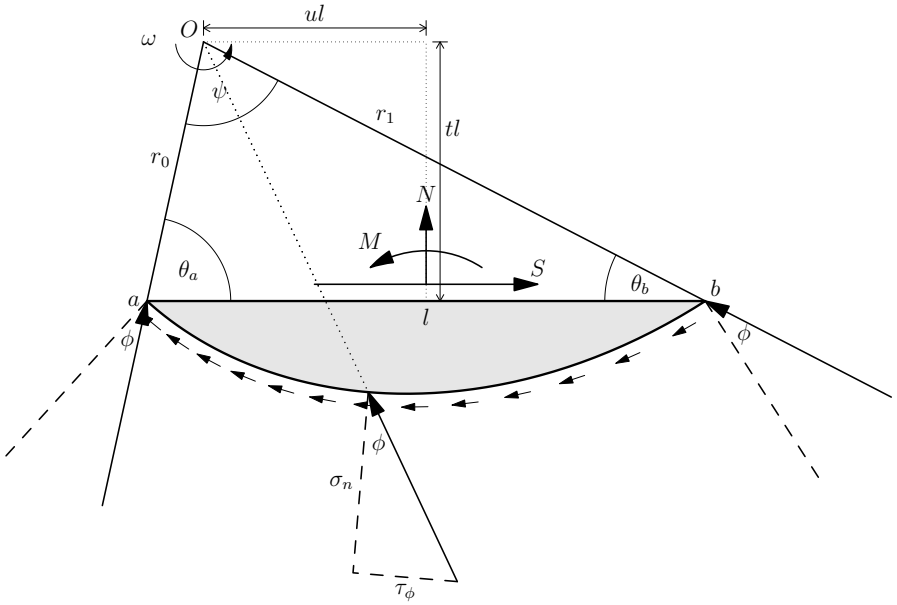

Figure 6: Geometry of log spiral ($\phi = 30^o$), with ω +ve (clockwise).

the requirement that *without yield being violated in only part of the domain* has been satisfied, neither has it been enforced to be at a magnitude lower than yield at some point on the line.

To generalise this point, it is necessary that f is convex in order to satisfy Theorem 4. Enforcement of yield in an average sense on a line for a non-convex yield surface will always require enforcement of a stress state less than yield somewhere on the line, unless all stresses on the line are equal to the average value, thus over-constraining the problem.

It should also be noted that an associative flow rule has not been invoked in this argument.

The nature of an upper bound equilibrium solution can now be clarified:

Theorem 5. *An upper bound solution based on slip-lines connecting pairs of*

nodes in a domain may be established by defining stress function parameters Φ*,* u*,* v *at these nodes, in equilibrium with external forces and maximising the live load while demonstrating that yield, defined by a convex surface, and determined using the slip-line end point nodal stress function values, is not violated in an average sense for each slip-line.*

Such a solution will implicitly satisfy all equilibrium requirements throughout the domain. This follows from the stress-function formulation. A stress function may always be fitted to (legitimate) boundary conditions, implicitly satisfying equilibrium, and since the functions are defined only at points, no a-priori assumption about the nature of the stress field has been made. Hence maximization of the live load through free choice of stress function values at these points will always satisfy the requirement that an exhaustive search has been carried out of all possible equilibrium stress fields. Without any yield checks, a maximised stress function will be a true upper bound, but will result in an infinite collapse load. For a useful upper bound it remains to enforce yield in part or all of the domain. This may be illustrated through a series of examples in Section 3, beginning with translational mechanisms and then considering rotational mechanisms. For sake of simplicity these examples will assume no body forces are acting, although inclusion of body forces is straightforward.

2.5. Implications

As discussed in Section 2.2, the stress function interpretation of the equilibrium form of the upper bound theorem demonstrates that for any analysis, equilibrium is implicitly guaranteed regardless of how many equilibrium

equations are employed. Equilibrium equations in the classical rigid-block analysis method are simply used to determine values of forces/moments that can be used to check that yield is not violated in an average sense along specific rigid block boundaries or to ensure equilibrium with external forces.

For example, the simple translational analysis presented in Figure 2, does not explicitly consider moment equilibrium. Similarly, for some problems, not all translational equilibrium checks are directly considered. Consider for example the sliding of a rigid block on a rigid horizontal surface with a cohesive interface. It is only necessary to utilise horizontal equilibrium to establish the failure load. This does not indicate that vertical equilibrium is not satisfied. It is simply that the forces associated with vertical equilibrium are not considered in the stability check. The following corollary to Theorem 5 may thus be stated:

Corollary 1. *(to Theorem 5) - An upper bound solution based on a rigid-block equilibrium analysis and in equilibrium with external forces will implicitly satisfy all equilibrium requirements throughout the domain. It is not necessary to check equilibrium is satisfied, but equilibrium equations may be used to determine forces and moments acting in the system in order to apply yield constraints in part of the domain.*

It may also be observed that the apparent assumption of yield on a 'slip-line' in equilibrium upper bound calculations follows on from the maximization requirement, rather than being an inherent assumption of the analysis. Hence, while the use of the term 'slip-line' presupposes slip and yield, such lines are perhaps better termed 'rigid block interface lines'.

It is also important to note that maximization is a necessary requirement

of an equilibrium upper bound computation, which renders it less straightforward to use than the kinematic case, especially for complex problems. In the kinematic case, minimization will generate a better upper bound solution, but non-minimized solutions will still be upper bounds.

3. Application examples

3.1. Translational mechanism analysis

3.1.1. Yield function

For a straight line, the centre of rotation is at infinity, $\psi \to 0$; hence, referring to Figure 6, $u/t \to \tan\phi$, M and M_S become negligible and equations 33 and 34 reduce to the familiar form of:

$$S \leq K - N\tan\phi \tag{36}$$

and when the shear stresses are reversed:

$$S \geq -K + N\tan\phi \tag{37}$$

where:

$$K = \int_a^b k.dl \tag{38}$$

Thus translational mechanisms formed of straight slip-lines are sufficient to give an upper bound solution, though not necessarily an optimal one. Only variables u and v need to be set at the end points of slip-lines in order to provide suitable values of S and N, that satisfy equations equation (36) and equation (37) and the boundary conditions. However Φ can take on any

value at the slip-line end points. It is only its gradient that is defined by u and v. Thus while moment equilibrium is implicitly satisfied, yield may occur along curved slip-lines since these are not checked.

3.1.2. Free body diagram solution (force based)

Before deriving a stress function based solution, it is useful to first derive a classical force based solution, where the slip-lines are pre-defined.

In a set of free body diagrams, yield is usually assumed on each line and generally the direction of action of the shear force is chosen by inspection (as it is typically obvious).

However, to generate a valid upper bound, it is necessary to set all the shear directions such that they maximise the load. Sometimes this is not intuitive as has been shown in Appendix B.

Returning to the simple indentation problem in Figure 1 and revisiting the analysis given in equation (8), this should therefore be rewritten as:

$$\max V = \sqrt{2}S_A + S + N = \sqrt{2}S_A + 2S + \sqrt{2}S_B \tag{39}$$

where:

$$-\sqrt{2}kL \leq S_A \leq \sqrt{2}kL \tag{40}$$

$$-kL \leq S \leq kL \tag{41}$$

$$-\sqrt{2}kL \leq S_B \leq \sqrt{2}kL \tag{42}$$

Equations 40 to 42 can be conveniently rewritten as follows:

$$S_A = \kappa_A \sqrt{2} kL \tag{43}$$

$$S = \kappa kL \tag{44}$$

$$S_B = \kappa_B \sqrt{2} kL \tag{45}$$

where $-1 \leq \kappa \leq 1$.

$$\max \frac{V}{kL} = 2\kappa_A + 2\kappa + 2\kappa_B \tag{46}$$

The result, by inspection, is clearly the same as given in equation (8), i.e. $V = 6kL$, where $\kappa_A = \kappa = \kappa_B = 1$..

In this problem there are 3 unknowns and 3 equations (43 to 45). If the value of κ on each line is chosen by inspection then the problem is thus statically determinate and thus there is only one value computed in equation (39) and the maximization process is redundant. This is true in general for any translational problem. Thus the implicit maximization is not seen in typical equilibrium calculations.

In general, mechanisms composed of triangles and/or quadrilaterals are statically determinate. Each additional quadrilateral will normally share two known boundaries. There are thus four additional unknowns (S and N twice), but two additional equilibrium equations and two additional yield equations relating S and N.

3.1.3. Stress function for two wedge indenter problem

The above calculation was carried out using values of the forces on discontinuities rather than the stress function variables at nodes. This is more intuitive for hand calculation purposes. However having done this, it can be examined directly with reference to stress function variables, given a statically determinate problem. The general procedure is as follows:

1. Set an arbitrary reference (Φ, u, v) triple (all calculations are relative).
2. Determine values of (Φ, u, v) at other nodes on loaded/free boundaries using the boundary conditions.
3. Determine values of (Φ, u, v) at internal nodes so that yield is not violated on any designated line. In simple cases maximum values can be taken on each line with shear direction determined intuitively.
4. Extract collapse load from values of (Φ, u, v) at ends of relevant boundaries.

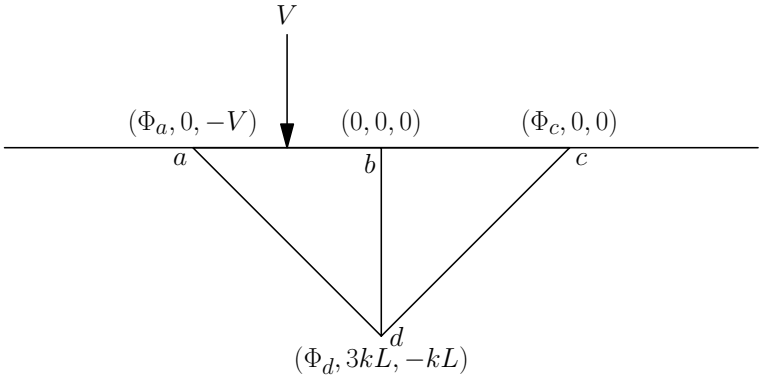

Figure 7: Two wedge solution for indenter problem showing u and v values

To solve the problem in Figure 1 it is necessary only to set the value of

u and v since only straight lines (translational) cases are being considered. Proceed as follows (with reference to the points a, b, c, and d in Figure 7):

1. Set an arbitrary reference of $(u_b, v_b) = (0, 0)$ at the origin (b).
2. Noting boundary conditions on bc, $N = T = 0$, gives $(u_c, v_c) = (0, 0)$. On ab, $N = -V = -(v_b - v_a)$ and $T = 0 = -(u_b - u_a)$, thus $(u_a, v_a) = (0, -V)$.
3. Invoke yield on bd, dc and da. Yield on bd requires $S = -(v_b - v_d) = -kL$, hence $v_d = -kL$. yield on dc requires $S = \frac{\sqrt{2}}{2}(-(u_c - u_d) - (v_c - v_d) = -\sqrt{2}kL$, hence $u_d = 3kL$. Yield on da requires $S = \frac{\sqrt{2}}{2}(-(u_a - u_d) - (v_a - v_d) = -\sqrt{2}kL$, hence $v_a = -6kL$.
4. Extract collapse load $V = -v_a = 6kL$.

It is clear that equilibrium has not explicitly been checked at any point. Stress function values were simply set in order to not violate yield or to satisfy surface boundary conditions.

It is now instructive to consider the nature of an equilibrium stress field that generates this upper bound solution. While it is possible to fit an infinite number of fields to these nodal values, here a simple piecewise cubic equation is chosen to represent the stress function that provides the nodal values in Figure 7. Taking the origin at b and $L = 1$, gives the equations as follows:

$$\Phi = (xy^2 + px^2 - 1.5y^2 - qx - 0.5q)k \tag{47}$$

$$u = \frac{\partial \Phi}{\partial y} = (2xy - 3y)k \tag{48}$$

$$v = -\frac{\partial \Phi}{\partial x} = (-y^2 - 2px + q)k \tag{49}$$

where $p = 0$, $q = -6$ for $x \leq -1$, $p = -3$, $q = 0$ for $-1 \leq x \leq 0$ and $p = q = 0$ for $x \geq 1$. The terms in q are not strictly necessary, but maintain a smooth stress function across the $x = -1$ and $x = 0$ lines. The stress function itself is plotted in Figure 8, and the stresses themselves are given by:

$$\sigma_x = \frac{\partial^2 \Phi}{\partial y^2} = (2x - 3)k \tag{50}$$

$$\sigma_y = \frac{\partial^2 \Phi}{\partial x^2} = 2pk \tag{51}$$

$$\tau_{xy} = \tau_{yx} = -\frac{\partial^2 \Phi}{\partial x \partial y} = -2yk \tag{52}$$

The states of stress at key points a, b, c and d are plotted as Mohr's circles in Figure 9. Since there is a stress discontinuity down the y-axis, circles are plotted at b and d on the left hand (l) and right hand (r) sides of the discontinuity.

It is clear by inspection that yield is violated at points b and d (and will be at many other locations); however by considering the dashed lines passing through the poles of the circles, it is also clear how the upper bound solution is achieved. The shear stress on slip-line ad at a is $0.5k$, and at d it is $1.5k$. Given the chosen stress function there is a linear variation of shear stress along the line ad and thus the average stress is k, satisfying the upper bound yield constraint on this line. The same can be seen for line cd.

For line bd, the shear stress varies from $0k$ at b to $2k$ at d. Again the average stress is k as required.

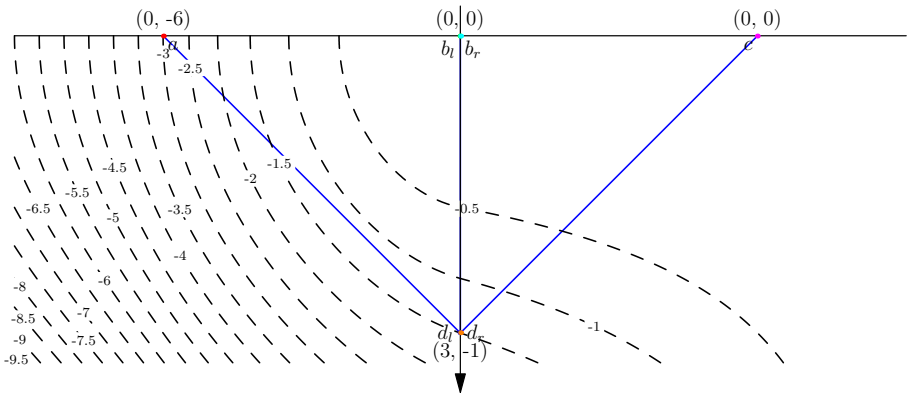

Figure 8: Two wedge stress function contours (dashed black lines) and slip-lines (solid blue lines) for $kL = 1$. Collapse load $= 6kL$.

3.1.4. Stress function for incomplete mechanism

Here the scenario where the line bd is omitted from the upper bound yield check is considered. In terms of shear forces on each line, equation (39), S is unbounded and so the maximum value of V is infinite. For the derivation of an example stress function, this will be considered equivalent to assuming the middle line has shear strength nk where $n \to \infty$. The results (presented in Appendix D) show that, while Mohr's circles at key points become infinite, resulting in an infinite load capacity, the averaged shear stress (shear stresses vary from negative to positive) along the checked discontinuities remains finite and equal to the yield stress.

3.1.5. Stress function for Prandtl mechanism

The preceding stress function solutions considered above clearly violates yield at many points within the stress field. It is of interest to examine the known true solution in the same context that was derived by Prandtl (1920).

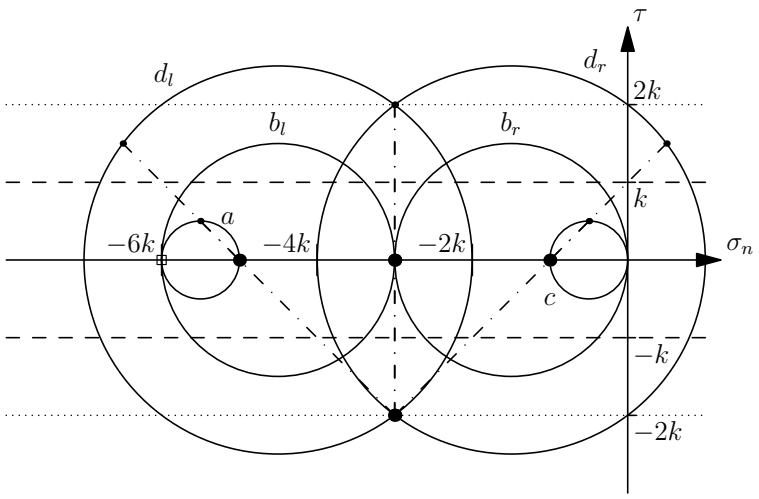

Figure 9: Two wedge stress function. Corresponding Mohr's circles. Poles of circles are marked by a large solid circle. Stress states on slip-line end points are marked by a small solid circle. Collapse stress $-6k$ indicated by hollow square.

For simplicity only half the problem will be considered (i.e. a semi-infinite indenter on the negative x-axis is considered. The stress function for the Prandtl problem is given as follows:

430

For $\tan^{-1}(-y/x) < 45^o$:

$$\Phi = -ky^2 \tag{53}$$

For $45^o < \tan^{-1}(-y/x) < 135^o$:

$$\Phi = k(x^2 + y^2)\left(\tan^{-1}(y/x) - 0.5 + 0.25\pi\right) \tag{54}$$

For $\tan^{-1}(-y/x) > 135^o$:

$$\Phi = 0.5k(-\pi y^2 - (2 + \pi)x^2) \tag{55}$$

The stress function itself is plotted in Figure 10 together with the Prandtl slip-line pattern. As before, the states of stress at key points a, b, c and d are plotted as Mohr's circles in Figure 11.

While Mohr's circles are plotted only at 6 locations, the lack of yield violation indicated extends across the whole domain. All circles have diameter $2k$. The angular positions of b about O are now significant and these were selected to be at $\pm 45^o$ to O. Hence they share the same stress state as either a or c.

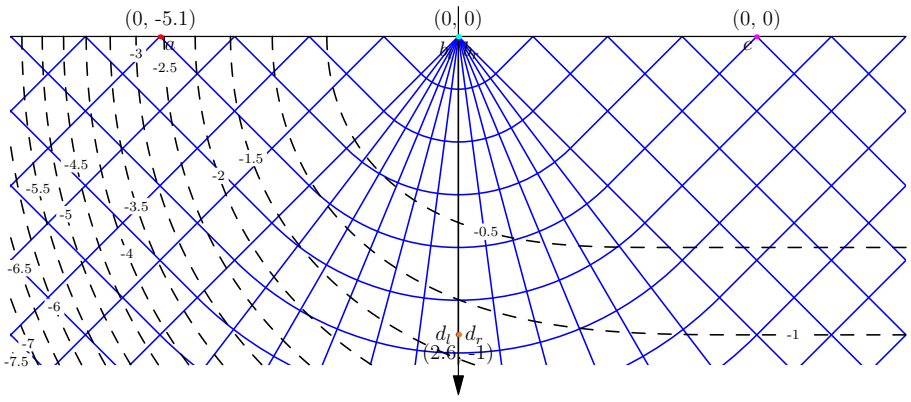

Figure 10: Prandtl solution stress function contours (dashed black lines) and slip-lines (blue solid lines) for $kL = 1$. Collapse load $= 5.14kL$.

3.2. Rotational mechanism analysis

While the translational analysis is relatively straightforward and often involves statically determinate problems, the same is not generally true when rotational mechanisms are involved. For a Tresca material with zero friction, the slip-lines will take the form of arcs of circles and the normal force will not affect the yield function.

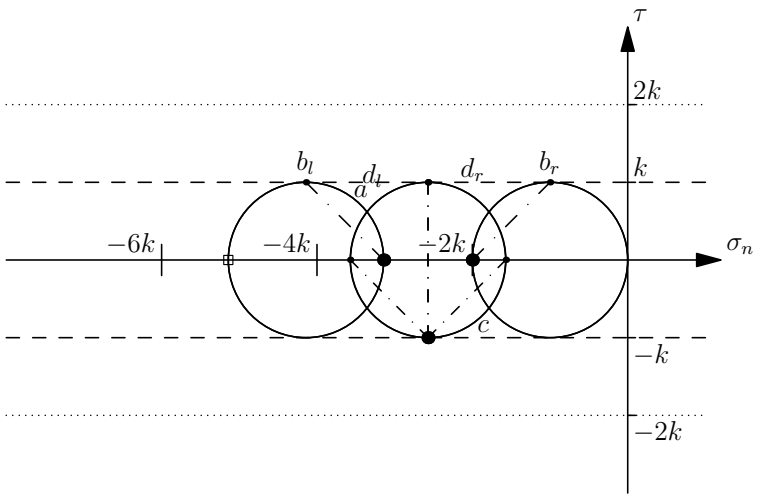

Figure 11: Prandtl solution stress function and corresponding Mohr's circles. Poles of circles are marked by a solid circle. Stress states on slip-line end points are marked by a small solid circle. Collapse stress $-5.14k$ indicated by hollow square.

3.2.1. Yield condition for curved slip-line

In Figure 6, under conditions of zero friction, $r = r_0 = r_1$, $u = 0$, and following equation (33), the yield condition can be written for an arc:

$$-\psi r^2 k \leq Sr\cos(\psi/2) + M \leq \psi r^2 k \tag{56}$$

where ψ is positive if O lies on the left hand side of ab and where M is positive bending towards a. This can be expressed as an equality as follows, where $-1 \leq \kappa \leq 1$:

$$M = \kappa\psi r^2 k - Sr\cos(\psi/2) \tag{57}$$

3.2.2. Single arc rotational solution

A simple statically determinate solution will first be considered. For a simple single arc rotational solution to the indentation problem (with reference to the nodal positions shown in Figure 7), where the centre of rotation lies on a vertical line through point b, and the arc starts at a and ends at c, it can be shown that the (Φ, u, v) values along the surface at a, b and c must be $(-p/2, 0, -p)$, $(0, 0, 0)$ and $(0, 0, 0)$ respectively where p is the normalised collapse load. $p = 2\pi k$ for a semi-circular arc and $p = 5.52k$ for the optimal rotational mechanism where $\psi = 134^o$ (Powrie, 2013).

A simple stress function that fits this is as follows:

For $x > 0$,

$$\Phi = -0.25py^2k \tag{58}$$

For $x < 0$:

$$\Phi = (-0.5px^2 - 0.25py^2)k \tag{59}$$

Consider the Mohr's circles as shown in Figure 12. It can be shown that the integral of the shear stress along the arc gives the expected moment M:

$$\frac{M}{kL^2} = \frac{\psi}{4\sin^2(\psi/2)} \tag{60}$$

3.2.3. Two wedge solution involving yield on rotational slip-lines

Now the two wedge problem will be analysed, where the lines are now treated as chords and where the potential for rotation about each chord

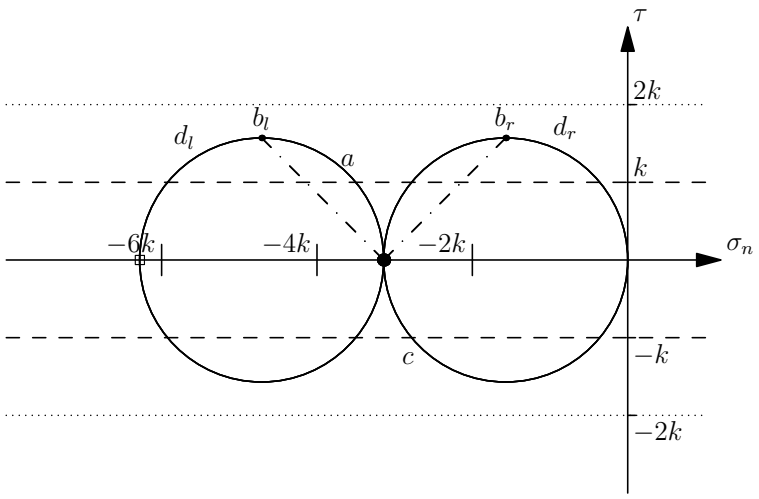

Figure 12: Mohr's cricles for single arc solution for indentation problem. Poles of circles are marked by a large solid circle. Stress states on slip-line end points are marked by a small solid circle. Collapse stress $-6.28k$ indicated by hollow square.

is considered. Moments are now also considered, leading to the free body diagrams depicted in Figure 13. (Note, S is drawn in Figure 13 in the opposite direction to Figure 2, in order to be consistent with the sign convention in Figure 6; similarly the normal force directions are reversed.) As before a solution invoking forces on chords rather than stress functions at nodes will first be examined.

Taking moments about A gives:

$$M_A + 0.5SL + M = 0 \tag{61}$$

Taking moments about B gives:

$$M_B + 0.5SL = M \tag{62}$$

Consideration of yield, equation (57), gives the following relationship be-

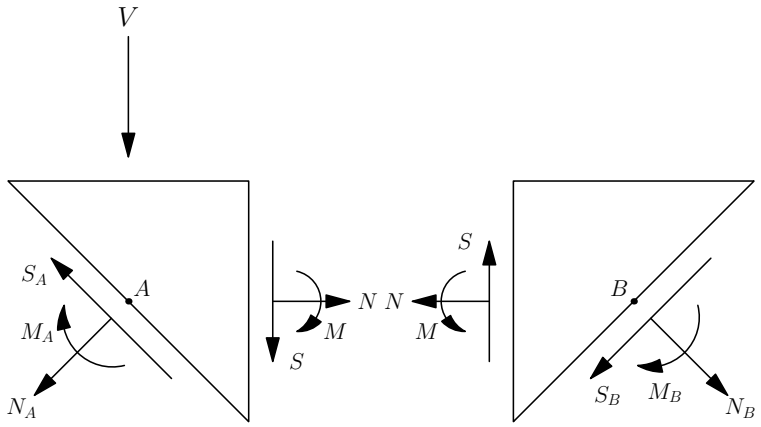

Figure 13: Free body diagrams for mechanism depicted in Figure 1

tween M and S:

$$M = \kappa\psi r^2 k - xS \tag{63}$$

where,

$$\cos(\psi/2) = x/r \tag{64}$$

480 and where ψ and x may be positive or negative. Also

$$M_A = \kappa_A \psi_A r_A^2 k - x_A S_A \tag{65}$$

$$M_B = \kappa_B \psi_B r_B^2 k - x_B S_B \tag{66}$$

Substituting

$$\kappa_A \psi_A r_A^2 k - x_A S_A + 0.5SL + \kappa\psi r^2 k - xS = 0 \tag{67}$$

$$(\kappa_A \psi_A r_A^2 + \kappa \psi r^2)k - x_A S_A = -(0.5L - x)S \tag{68}$$

$$S_A = \frac{(\kappa_A \psi_A r_A^2 + \kappa \psi r^2)k + (0.5L - x)S}{x_A} \tag{69}$$

At B:

$$\kappa \psi_B r_B^2 k - x_B S_B + 0.5SL = \kappa \psi r^2 k - xS \tag{70}$$

$$(\kappa_B \psi_B r_B^2 - \kappa \psi r^2)k - x_B S_B = -(0.5L + x)S \tag{71}$$

$$S_B = \frac{(\kappa_B \psi_B r_B^2 - \kappa \psi r^2)k + (0.5 + x)S}{x_B} \tag{72}$$

Based on equation (8), the overall force V is given by:

$$\max\ V = \sqrt{2}S_A - 2S + \sqrt{2}S_B \tag{73}$$

Hence

$$\max\ V = \sqrt{2}\frac{(\kappa_A \psi_A r_A^2 + \kappa \psi r^2)k + (0.5L + x)S}{x_A} - 2S + \sqrt{2}\frac{(\kappa_B \psi_B r_B^2 - \kappa \psi r^2)k + (0.5L - x)S}{x_B} \tag{74}$$

485 The above equation holds for any arbitrary choice of curved slip-lines. However in general since S is unconstrained, most solutions will yield infinite (locked) results. Finite solutions can only be obtained if the corresponding kinematic problem is kinematically compatible, i.e. only very specific sets of curves will give finite solutions.

To generate a kinematically compatible set of curves for this problem, first centres of rotations for block A and block B are selected as appropriate (this is a free choice). Example values are shown in Figure 14. Using the fact that the centre of rotation of the interface of two blocks must lie on a line joining the centres of rotation of the blocks (see e.g. Smith and Gilbert 2013), the centre of curvature of the slip-line bd is fixed at $(-2.5L, -0.5L)$. The parameters to be used in equation (74) are shown in Case 1 of Table 1. To maximise V, $\kappa_A = 1$ and $\kappa_B = 1$, while $\kappa = -1$ if $x_A > x_B$ and $\kappa = 1$ if $x_B > x_A$. It can be seen that the multiplier on S is zero and V is therefore a constant value and so the maximization process has no effect.

Case 2 of Table 1 gives the case when the centre of curvature of slip-line bd is moved, in this case to $(-2L, -0.5L)$ so that the mechanism is not compatible. In this case V is a function of S and since S can take any arbitrary value, the maximum value of V is infinity.

Case 3 models two slip-lines linking nodes b and d, where the centres of curvature are set at $(-2L, -0.5L)$ and $(-3L, -0.5L)$. The use of two lines enables kinematic compatibility (Smith and Gilbert, 2015). Here the combination does restrict the maximization process giving a finite result. Having two slip-lines (1 and 2) connecting a single pair of nodes, leads to a simultaneous equation with two versions of equation (63) giving:

$$S = \frac{\kappa_2 \psi_2 r_2^2 kL - \kappa_1 \psi_1 r_1^2 kL}{x_2 - x_1} \tag{75}$$

V is still maximised if $\kappa_1 = \kappa_2 = -1$, and the result is now finite due to the constrained value of S. The two curved slip-lines linking node b to d bracket the Case 1 slip-line, and this generates a result that is only marginally

larger than Case 1. The reader is referred to Smith and Gilbert (2015) for further details on theory relating to multiple curved slip-lines that link the same points.

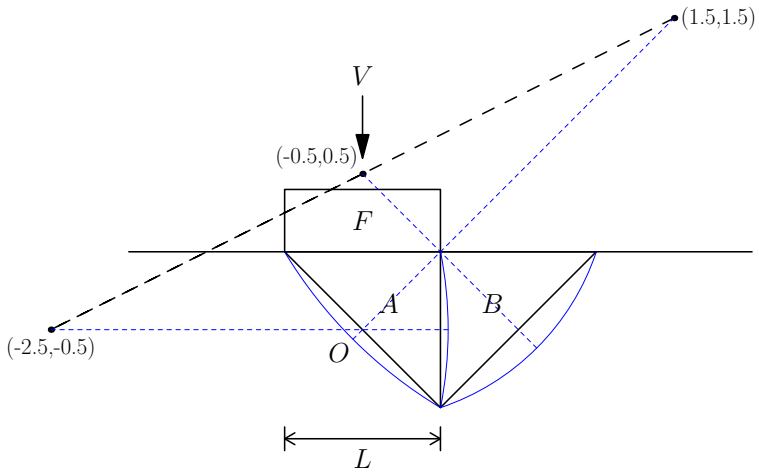

Figure 14: Postulated failure mechanism. Slip-lines indicated using solid blue lines. Radii from centre of rotation to arc centre indicated using dashed blue lines.

Table 1: Equilibrium forces and stress function values in upper bound calculations for two-wedge cases considered in Figure 14 (ψ is given in radians). *= unconstrained.

Case	1	2	3
x_A/L		$2\sqrt{2}$	
r_A/L		2.9154	
ψ_A		0.4900 (28.1^o)	
κ_A		1	
x/L	2.5	2	2 & 3
r/L	2.5495	2.0616	2.06 & 3.04
ψ	0.3947 (22.6^o)	0.4900 (28.1^o)	0.4900 & 0.3303
κ	-1	-1	-1
x_B/L		$\sqrt{2}$	
r_B/L		1.5811	
ψ_B		0.9273 (53.1^o)	
κ_A		1	
S_A	$0.5652kL - 0.5\sqrt{2}S$	$0.7362kL - 0.375\sqrt{2}S$	$1.2522kL$
S	*	*	$-0.9729kL$
S_B	$3.4538kL + 1.5\sqrt{2}S$	$3.1117kL + 1.25\sqrt{2}S$	$1.3917kL$
M_A	$2.5661kL^2 + 2SL$	$2.0823kL^2 + 1.5SL$	$0.6229kL$
M	$-2.5661kL^2 - 2.5SL$	$-2.0823kL^2 - 2SL$	$-0.1365kL$
M_B	$-2.5661kL^2 - 3SL$	$-2.0823kL^2 - 2.5SL$	$0.3500kL$
V	$5.6836kL + 0S$	$5.4417kL - 0.25S$	$5.6849kL$
Ψ_a	$-2.8418kL^2$	$-2.7209kL^2 + 0.125SL$	$-2.8425kL^2$
u_a	0	0	0
v_a	$-5.6836kL$	$-5.4417kL + 0.25SL$	$-5.6849kL$
Ψ_d	$-5.0083kL^2 - 3.5SL$	$-4.2826kL^2 - 2.75SL$	$-1.6070kL^2$
u_d	$4.8844kL + 2S$	$4.4006kL + 1.5S$	$2.9411kL$
v_d	S	S	$-0.9729kL$

Stress function values may be determined using the same process as outlined in Section 3.1.3. This gives values of Ψ, u, and v for each case as shown in Table 1, where $(\Psi_b, u_b, v_b) = (\Psi_c, u_c, v_c) = (0, 0, 0)$.

4. Generation of a lower bound solution from an upper bound solution

It can be seen that a stress function based upper bound solution satisfies many of the requirements of an associative lower bound in that the stress field is in equilibrium everywhere and also in equilibrium with external forces. However yield may be violated in certain locations. The potential of the upper bound stress function approach then becomes apparent; it is generally possible to scale any upper bound stress field in order to bring the largest Mohr circle within the yield envelope. The quality of the results clearly depends on the quality of the stress field chosen.

This may be illustrated through consideration of the single arc solution in Section 3.2.2 that is a remarkably simple solution reminiscent of the simple two zone, one stress value discontinuity lower bound solution for an indenter where the Mohr's circle (see Figure 12) has radius k on both sides of the y-axis. For this case, the loads can be scaled back to $V = 4k$, which brings all the Mohr's circles within the yield envelope.

This scaling is straightforward for single load problems such as the indentation problem. For more complex problems involving friction or material self weight, the scaling of a single external load is generally not possible. However an alternative lower bound can be proposed by simply increasing the yield envelope until all Mohr's circles are within that envelope. A solu-

tion as in this case can be given as $V = 5.52k$ and has a definite status for material strengths of k and $5.52k/4$. The system will definitely fail with the former strength and will definitely not fail with the latter strength.

5. Discussion

While this paper has focused on hand calculations and pre-determined simple layouts of slip-lines, the principles can be applied to any number of nodes and any number of slip-lines linking these nodes (which may cross over each other any number of times). This, however requires a numerical approach and is the background to the Discontinuity Layout Optimization (DLO) method, Smith and Gilbert (2007) and Smith and Gilbert (2013) which is able to generate upper bound solutions of high accuracy. The implication is that constraining yield in an average sense along lines is efficient and requires no finite element or meshless method basis function.

A DLO solution essentially defines the stress function field as point and gradient values on a grid of nodes in such a way that the basis function is not predefined and is thus able to deal with any problem type and stress field rather than requiring one that can potentially lead to a poor solution. Using efficient numerical optimization, it finds a set of nodal stress function values that maximises the applied load while ensuring yield is not violated on all (or selected) lines connecting every pair of nodes. As the number of lines and nodes approaches infinity, then the solution will implicitly approach the true associative solution as it will tend towards the form of a lower bound solution, where yield is checked everywhere. Figure 15 illustrates the increasing accuracy of the DLO solution to the Prandtl punch problem as

the number (n) of nodes increases (results after Smith and Gilbert 2013). The number of lines checked is given by $n(n-1)/2$. The plotted lines are those on which yield is occurring in the solution.

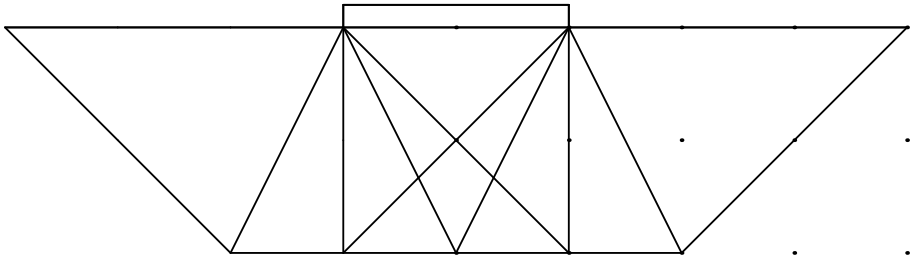

(a)

$n_d/B = 2$, $V/kB = 5.667$, $\epsilon = 10.2\%$

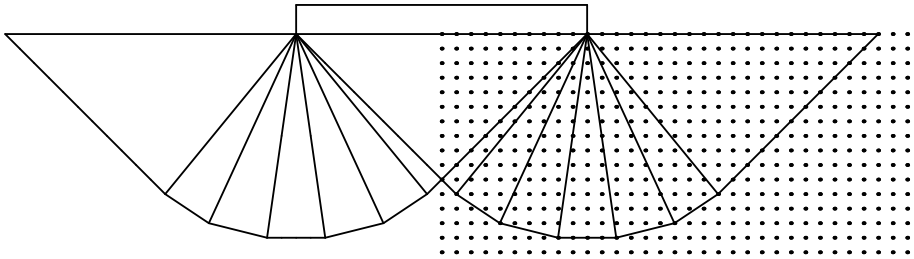

(b) $n_d/B = 20$, $V/kB = 5.163$, $\epsilon = 0.42\%$,

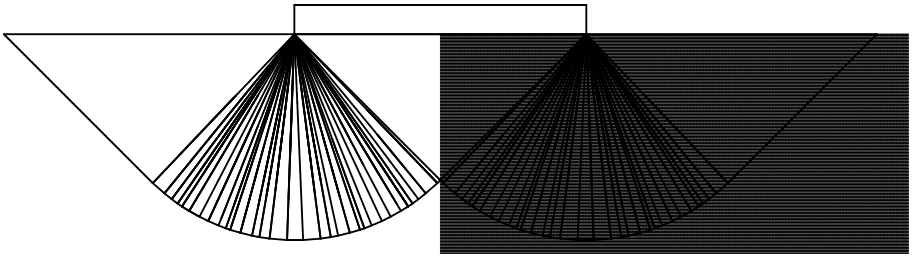

(c)

$n_d/B = 200$, $V/kB = 5.143$, $\epsilon = 0.03\%$

(node dot size reduced for clarity).

Figure 15: DLO solutions showing influence on the collapse load V of the number of nodal divisions n_d used to discretize a Prandtl punch of width B, bearing on a material of strength k. ϵ gives percentage difference relative to exact solution of $(2+\pi)kB$. Distribution of nodes indicated on right side of figure.

Other workers, e.g. Canh et al. (2016), have also proposed stress function based mesh free approaches for lower bound solutions which appear promising, and with sufficient discretisation, basis function based methods (mesh and mesh free) can fit even the most complex stress function. A particular advantage of the line based approach is that it can capture single line solutions such as that in Section 3.2.2 elegantly with only a few nodes, whereas a finite element or meshless method based approach would require significant refinement. It would appear that there is significant promise in establishing a hybrid approach, where the advantages of each can be combined.

.

As noted previously, translational problems are generally statically determinate. From the stress function perspective, the addition of two faces to construct a new quadrilateral adds two unknowns (u, v) which is balanced by the addition of two yield equations . However for rotations three unknowns (Φ, u, v) are added but only two yield equations, thus introducing an extra degree of freedom, which can lead to infinite (unbounded) solutions unless the slip-lines are chosen to eliminate this. It turns out, in the kinematic context, that this requires kinematic compatibility conditions to be met.

If the shear direction is not chosen to maximise the collapse load, then a type of non-associative solution will be found. However, this solution has no strict status. The corresponding stress field is likely to violate yield in locations other than the tested slip-lines, so while a maximised solution is a guaranteed upper bound if an associative material is involved, this status is lost if the maximization step is omitted. This thus clarifies the issue raised by Michalowski (1989) concerning the difference between the 'limit equilibrium'

form and the energy balance limit analysis form of the upper bound theorem. It is noted further, that for a non-associative 'limit equilibrium' solution to be valid, it has to demonstrate both that yield is not violated at any point and that yield occurs on slip-lines that form a mechanism.

For simplicity, this paper has focused on 2D plane strain problems, however the methodology may be readily extended to 3D, using appropriate 3D stress functions e.g. Maxwell (1870), and slip-surfaces rather than slip-lines. Such an approach leads to a 3D equilibrium form of DLO such as presented by Hawksbee et al. (2013).

6. Conclusions

Equilibrium form of the upper bound

1. The equilibrium form of the upper bound theorem is the mathematical dual of the kinematic form. For a correct solution, maximization of the load must be carried out for any given set of rigid block boundaries to be a valid upper bound. The maximization process typically relates to an assumption of yield and choice of direction of shear force on any rigid block boundary.
2. The advantage of the kinematic approach is that it is often more straightforward than the equilibrium approach for hand calculations. The optimal solution is found from minimization. However if minimization is omitted the solution is still a valid upper bound. For a fixed geometry of mechanism the compatibility as determined from a hodograph determines the solution and minimization is not necessary/possible.

3. In contrast, for an equilibrium solution, maximization may not be omitted. However, for translational mechanisms, the shear direction is often obvious and the problem is typically statically determinate and so maximization may not explicitly be necessary.
4. Problems involving rotational mechanisms are typically not statically determinate and thus maximization must be explicitly carried out when working with the equilibrium form.
5. There is no immediately apparent need for a given arrangement of sliding blocks to form a kinematically compatible mechanism. However if there are insufficient sliding interfaces (constraints), or if they are not kinematically compatible, the limit load will be infinite (unbounded), corresponding to a kinematically locked sliding block configuration.
6. The 'limit equilibrium' (LE) approach differs from the equilibrium form of the upper bound in that it (a) does not enforce kinematic compatibility for the chosen mechanism and (b) does not enforce maximization of the load. If the shear force direction is chosen such that the load is not maximised then a type of non-associative solution has been found.

Stress functions

1. It is possible to formulate the equilibrium form of an upper bound rigid-block plane strain problem in terms of stress function parameters at the nodes connecting sliding interfaces. These parameters may be used to calculate shear forces S, normal forces N, and moments M, acting on straight lines connecting any node pair, which in turn may be used to check yield in an average sense.
2. Full rotational and translational equilibrium is implied in any upper

bound calculation. Equilibrium equations, as used in classical rigid block analysis, are used only to ensure equilibrium with external forces or to establish values of S, N, M on rigid block interfaces in order to check yield.

3. In principle it is possible to establish a continuum equilibrium stress field across the domain passing through the stress function values established at the nodes. However since yield is only checked on specific lines and in an average sense this results in a upper bound rather than lower bound solution.

4. An infinite number of stress function fields may be fitted to these nodal values. Suitable fields can be scaled to ensure yield is nowhere violated and thus used to obtain a lower bound solution.

5. For simple problems the stress function formulation adds complexity which is unnecessary for a solution unless a lower bound is also required. The main benefit is the rigour that the theory adds to the interpretation of an equilibrium analysis. For more complex problems involving e.g. complex geometry, non-linear yield functions, 3D analysis etc., solutions are best addressed numerically using e.g. the stress function approach implicit in the discontinuity layout optimization (DLO) method.

Acknowledgements

This work was supported by the UK Engineering and Physical Sciences Research Council (EPSRC), under grant reference EP/T001305/1. Initial work in the area of this study was undertaken whilst the second author was

in receipt of an EPSRC Advanced Research Fellowship, grant GR/S53329/01.

References

Airy, G., 1863. On the strains in the interior of beams. Phil. Trans. Roy. Soc. 153, 49–71. Https://doi.org/10.1098/rstl.1863.0004.

Calladine, C., 1985. Plasticity for Engineers. Ellis Horwood.

Canh, V., Phuc, L., Hoa, T., 2016. Airy-based equilibrium mesh-free method for static limit analysis of plane problems. Vietnam Journal of Mechanics, VAST 38, 167–179.

Chakrabarty, J., 2006. Theory of plasticity. 3rd ed., Oxford: Butterworth-Heinemann.

Charnes, A., Lemke, C.E., Zienkiewicz, O.C., 1959. Virtual work, linear programming and plastic limit analysis. Proceedings of the Royal Society of London. Series A, Mathematical and Physical Sciences 251, 110–116.

Chen, W., 1975. Limit Analysis and Soil Plasticity. Developments in Geotechnical Engineering 7, Elsevier.

Ciria, H., Peraire, J., Bonet, J., 2008. Mesh adaptive computation of upper and lower bounds in limit analysis. International Journal for Numerical Methods in Engineering 75, 899–944.

Collins, I., 1969. The upper bound theorem for rigid-plastic solids generalised to include coulomb friction. J. Mech. Phys. Solids 17, 323–338.

Drucker, D., Prager, W., Greenberg, H., 1952. Extended limit design theorems for continuous media. Quart. Appl. Math. 9, 381–389.

Gilbert, M., Casapulla, C., Ahmed, H., 2006. Limit analysis of masonry block structures with non-associative frictional joints using linear programming. Comput. & Struct. 84, 873–887.

Gvozdev, A., 1938. The determination of the value of the collapse load for statically indeterminate systems undergoing plastic deformation, in: Proceedings of the Conference on Plastic Deformation, Acad. of Science, USSR. pp. 19–33. English Translation in Int. J. Mech. Sci. , 1960, Vol 1, pp. 322-355.

Hawksbee, S., Smith, C., Gilbert, M., 2013. Application of discontinuity layout optimization to three-dimensional plasticity problems. Proc. R. Soc. A 469.

Hill, R., 1951. On the state of stress in a plastic-rigid body at the yield point. Phil. Mag. 42, 868–875.

Johansen, K.W., 1962. Yield-line theory. Cement and Concrete Association, London, United Kingdom.

Johnson, W., Mellor, P., 1962. Plasticity for Mechanical Engineers. D, Van Nostrand Company.

Maxwell, J., 1870. On reciprocal figures, frames, and diagrams of force. Edinburgh Royal Soc. Trans 26, 1–40.

Michalowski, R., 1989. Three-dimensional analysis of locally loaded slopes. Geotechnique 39, 27–38.

Nielsen, M., Hoang, L., 2011. Limit Analysis and Concrete Plasticity, 2nd ed., CRC Press, Boca Raton, 1999,. CRC Press.

Powrie, W., 2013. Soil Mechanics: Concepts and Applications. 3rd ed., CRC Press.

Prandtl, L., 1920. Uber die harte plastischer korper. Math. Phys. Kl. , 74–85.

Smith, C., 2012. Limit loads for a shallow anchor/trapdoor embedded in a non-associative coulomb soil. Géotechnique 62, 563–571.

Smith, C., Cubrinovskii, M., 2011. Pseudo-static limit analysis by discontinuity layout optimization: Application to seismic analysis of retaining walls. Soil Dyn. Earthq. Eng. 31, 1311–1323.

Smith, C., Gilbert, M., 2007. Application of discontinuity layout optimization to plane plasticity problems. Proc. R. Soc. A 463, 2461–2484. Doi:10.1098/rspa.2006.1788.

Smith, C., Gilbert, M., 2013. Identification of rotational failure mechanisms in cohesive media using discontinuity layout optimisation. Géotechnique 63, 1194–1208. Doi:10.1680/geot.12.P.082.

Smith, C.C., Gilbert, M., 2015. Modelling rotational failure in confined geometries using DLO. Proceedings of the Institution of Civil Engineers - Engineering and Computational Mechanics 168, 155–168.

Appendix A. Kinematic energy based analysis of punch problem

Analysis of the problem depicted in Figure 1 proceeds as follow. A compatible velocity field is first established using a hodograph, as shown in Figure A.16. The (rigid) indenter F is assumed to move with block A.

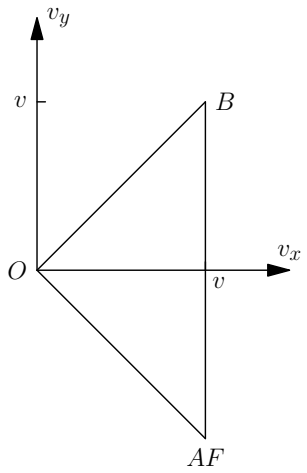

Figure A.16: Hodograph for mechanism depicted in Figure 1

730

The work equation (equating external work to internal energy dissipated) is as follows:

$$Vv = k(\sqrt{2}v\sqrt{2}L + 2vL + \sqrt{2}v\sqrt{2}L) = 6kvL \tag{A.1}$$

$$V = 6kL \tag{A.2}$$

Appendix B. Example of non-intuitive choice of shear direction in an equilibrium analysis

An example in the field of geotechnical engineering, where setting the shear direction to maximise the load in an equilibrium analysis is not necessarily intuitive can be found in Smith and Cubrinovskii (2011), where the Mononobe-Okabe pseudo-static analysis of active earth pressure on retaining walls subject to earthquake accelerations is considered. At large accelerations the 'limit equilibrium' solution of Mononobe-Okabe starts to deviate from the upper bound limit analysis solution, because the direction of shear (defined by the orientation of δ') on the wall/soil wedge interface reverses in the limit analysis equilibrium solution, in order to achieve the minimum load (for an active earth pressure problem, the smallest restraining force is sought). This is shown in Figure B.17, where, perhaps counter intuitively, the force would not normally be expected to act downwards. The 'limit equilibrium' solution may therefore be regarded as a potential non-associative solution, but has no specific status other than being greater than the associative solution (for the same mechanism).

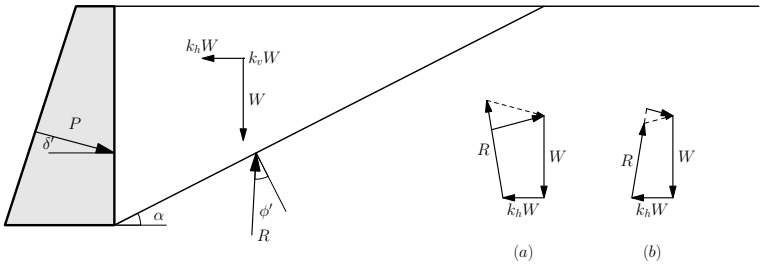

Figure B.17: Reversal of shear stress on soil/wall interface at high seismic accelerations. Smallest value of active force P and its angle of inclination depends on whether reaction force R is inclined (a) to the left, or (b) to the right of the vertical. The transition occurs when $\phi = \alpha$.

Appendix C. Stresses along a line

Appendix C.1. Shear stresses

The shear stress along a line (with direction cosines α and β) may be derived from the shear and normal stresses acting on the x and y planes as follows:

$$\tau = (-\sigma_x + \sigma_y)\alpha\beta + \tau_{yx}\alpha^2 - \tau_{xy}\beta^2 \tag{C.1}$$

$$\tau = -\frac{\partial u}{\partial y}\alpha\beta - \frac{\partial v}{\partial x}\alpha\beta - \frac{\partial u}{\partial x}\alpha^2 - \frac{\partial v}{\partial y}\beta^2 \tag{C.2}$$

Noting that:

$$du = \frac{\partial u}{\partial x}.dx + \frac{\partial u}{\partial y}.dy = \frac{\partial u}{\partial x}\alpha.dl + \frac{\partial u}{\partial y}\beta.dl \tag{C.3}$$

$$dv = \frac{\partial v}{\partial x}.dx + \frac{\partial v}{\partial y}.dy = \frac{\partial v}{\partial x}\alpha.dl + \frac{\partial v}{\partial y}\beta.dl \tag{C.4}$$

Hence:

$$\tau = -\alpha\frac{du}{dl} - \beta\frac{dv}{dl} \tag{C.5}$$

Appendix C.2. Normal stresses

The normal stress along a line (with direction cosines α and β) may be derived from the shear and normal stresses acting on the x and y planes as follows:

$$\sigma_n = \sigma_x\beta^2 + \sigma_y\alpha^2 - \tau_{xy}\alpha\beta - \tau_{yx}\alpha\beta \tag{C.6}$$

$$\sigma_n = \frac{\partial u}{\partial y}\beta^2 - \frac{\partial v}{\partial x}\alpha^2 - \frac{\partial v}{\partial y}\alpha\beta + \frac{\partial u}{\partial x}\alpha\beta + \Omega(\alpha^2 + \ \beta^2) \tag{C.7}$$

Hence:

$$\sigma_n = \beta\frac{du}{dl} - \alpha\frac{dv}{dl} + \Omega \tag{C.8}$$

Appendix C.3. Stress function

The stress function may be defined in terms of the integrals of u and v as follows:

$$\int d\Phi = \int \frac{\partial \Phi}{\partial x}.dx + \int \frac{\partial \Phi}{\partial y}.dy \tag{C.9}$$

$$\Phi = \int -v.dx + \int u.dy \tag{C.10}$$

Appendix D. Unbounded stress function solution for indentation problem

With reference to Figure 7, the assumption that the middle line ad has strength nk where $n \to \infty$. results in a more general form of equation (47) as follows:

$$\Phi = ((n+1)xy^2/2 + px^2 - (n+2)y^2/2 - qx - 0.5q)k \tag{B 1}$$

where $p = 0$, $q = -2(n+2)$ for $x \leq -1$, $p = -(n+2)$, $q = 0$ for $-1 \leq x \leq 0$ and $p = q = 0$ for $x \geq 1$.

The choice of $n = \infty$ results in Mohr's circles of infinite size and to an infinite load capacity. This is consistent with not having a kinematically

compatible mechanism defined. To illustrate the nature of the stress field, it is instructive to consider the case where $n = 2$ and extrapolate from there. The Mohr's circle plot is given in Figure D.18. Relative to Figure 9, circles b and d have increased in size, while circles a and c have reduced to points. However the average stress along lines ad and cd can still be seen to be k, while the average stress along bd is now $2k$. As n increases, circles b and d continue to increase in size while a and c also increase with the principal stress directions swapping over. This maintains the average stress along lines ad and cd constant at k, while allowing the applied load to increase to $2(n + 2)kL$.

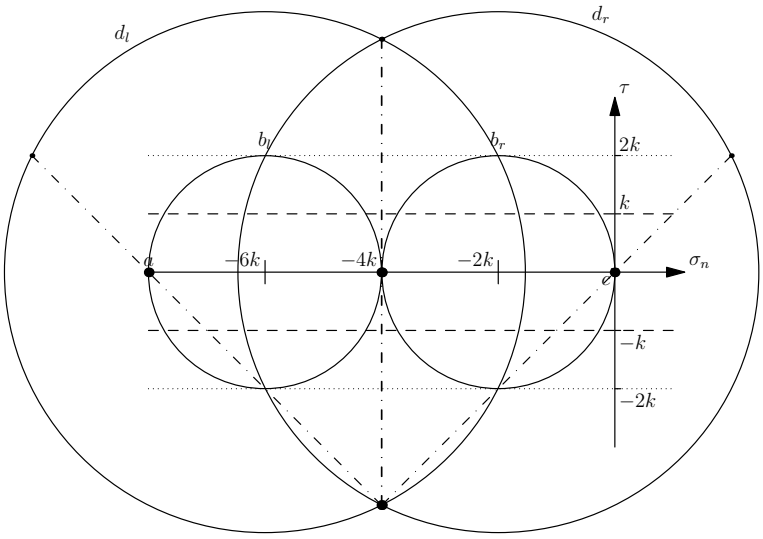

Figure D.18: Two wedge stress function with shear force $2kL$ on centre line. Note circles a and c have shrunk to points with zero diameter. Poles of circles are marked by a large solid circle. Stress states on slip-line end points are marked by a small solid circle.